Investigations of the Rear-End Flow Structures on a Sedan Car

Citation for the original published paper (version of record):

Kounenis, C., Bonitz, S., Ljungskog, E. et al (2016). Investigations of the Rear-End Flow Structures on a Sedan Car. SAE Technical Papers. http://dx.doi.org/10.4271/2016-01-1606

(article starts on next page)

Investigations of the Rear-End Flow Structures on a Sedan Car

Author, co-author (Do NOT enter this information. It will be pulled from participant tab in MyTechZone)

Affiliation (Do NOT enter this information. It will be pulled from participant tab in MyTechZone)

Abstract

The aerodynamic drag, fuel consumption and hence CO_2 emissions, of a road vehicle depend strongly on its flow structures and the pressure drag generated. The rear end flow which is an area of complex three-dimensional flow structures, contributes to the wake development and the overall aerodynamic performance of the vehicle.

This paper seeks to provide improved insight into this flow region to better inform future drag reduction strategies. Using experimental and numerical techniques, two vehicle shapes have been studied; a 30% scale model of a Volvo S60 representing a 2003MY vehicle and a full scale 2010MY S60.

First the surface topology of the rear end (rear window and trunk deck) of both configurations is analysed, using paint to visualise the skin friction pattern. By means of critical points, the pattern is characterized and changes are identified studying the location and type of the occurring singularities. The flow field away from the surface is then analysed using PIV measurements and CFD for the scale model and CFD simulations for the full scale vehicle. The flow field is investigated regarding its singular points in cross-planes and the correlation between the patterns for the two geometries is analysed.

Furthermore, it is discussed how the occurring structures can be described in more generalized terms to be able to compare different vehicle geometries regarding their flow field properties.

The results show the extent to which detailed flow structures on similar but distinct vehicles are comparable; as well as providing insight into the complex 3D wake flow.

Introduction

Reducing the fuel consumption is one of the important aspects in today's vehicle development. A decrease of the aerodynamic drag reduces the total driving resistance and contributes to a lower fuel consumption of the vehicle.

The aerodynamic drag for passenger vehicles is dominated by pressure drag. The flow field around the car is characterized by big separation regions, particularly the wake created at the rear end of the car. To improve the aerodynamic performance it is desired to reduce and optimise this area around the vehicle.

In order to optimise the shape towards an improved aerodynamic behaviour, it is of interest to understand the physics and driving forces which lead to the observed structures and phenomena.

Moreover, a language is required which allows to describe and characterise the flow in a more generic way, in order to compare different vehicle geometries.

In the past, a lot of research was carried out on different kinds of notchback and fastback geometries (often simplified bodies), for instance [1, 2, 3, 4, 5, 6, 7, 8, 9, 10, 11, 12, 13, 14]. The investigation of geometric parameters like the backlight angle, effective backlight angle, trunk deck length and the relation to each other give indications for an improved vehicle shape [9, 10, 11, 15, 16].
Another interesting observation is the occurrence of symmetric and asymmetric flow pattern for different notchback vehicle shapes (for instance [8, 9, 14]). Sims-Williams et al. [9] investigated the flow pattern for different generic notchback geometries and the connection between the backlight angle and the effective backlight angle. They found that the flow can be divided into three different groups: i) fully separated, ii) reattaching symmetric and iii) reattaching asymmetric. According to their work, the investigated S60 passenger car lies exactly on the transition between reattaching asymmetric and reattaching symmetric shapes. Flow visualisations will show that the observed pattern is symmetric.

Looking into the literature shows that many notchback like geometry studies were done on simplified shapes and generic bodies [2, 3, 5, 9, 10, 11, 12]. These investigations show that the flow field is different, as for instance vortices are different in size and position, but on the other hand main features like saddle points and foci are present in a similar way for the different geometries. As a result, these features could be used for a more generalised flow characterisation.

Flow field investigations on realistic modern car shapes are rare and detailed studies of the rear end flow field of realistic notchback vehicles are almost not present [6, 13]. Strangefeld et al. [13] investigated the flow characteristics of a 1/4 scale notchback DrivAer model. The flow over the rear window and the wake behind the model were investigated with PIV, but only in the centre plane. It was shown that the time-averaged wake consist of two counter rotating vortices which are closed by a 2D saddle point. In a later work Wieser et al. [14] presented surface data of the same DrivAer model, where it is shown that the flow pattern over the notchback rear end is asymmetric. However, more detailed information about the flow and wake structure in planes where the flow asymmetry occurs is not given.

The complexity of today's geometries requires more detailed studies. Curved rear end shapes and for instance the radius of the pillars could add an additional sensitivity onto the flow field and basic parameters as backlight angle and effective backlight angle are not sufficient to describe the structures. Therefore more independent characterisations are needed to describe and assess or characterise the flow.

One possibility for a more generic flow field description could be the investigation of singular points [17]. This method was already used in some publications, for instance in [4, 5, 6, 7, 8 17, 18]. Occurring separation lines, foci, saddles and nodes (on the surface and in planes) can be located accurately and build the skeleton for 3D structures. A step further could be to use these flow field characteristics for the comparison of different vehicle shapes. For instance as characteristic length scales.

This work will investigate two Volvo S60 notchback geometries; a 30% scale model from 2003 and a full scale car from 2010. These two test models provide differences at the rear end geometry but also in scale. Numerical and experimental methods were used to investigate the flow field and the surface flow patterns. The occurring singular points are studied and used to describe the flow patterns. This characterisation is then used to compare the pattern for the two investigated vehicles on the surface and at different cross planes.

Experimental Method

Test Vehicle

For this study, a 30% scale model of Volvo S60 (2003MY) sedan type car was used. The model carries all major engine bay components as well as a detailed underbody and can be seen in **Figure 1**. It has to be mentioned that the model differs only in a few minor details (mirrors, engine compartment components) and is close to production status in detail level. Additional information on the Volvo S60 model can be found in [19, 20, 21].
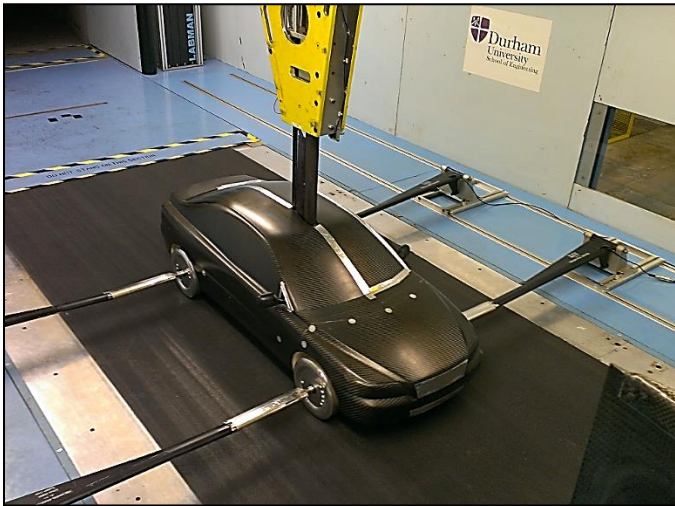

Figure 1: Volvo S60 30% model in the Durham University 2m² wind tunnel.

Wind Tunnel

The 2m² Durham University wind tunnel was used for all the experimental studies of the model scale vehicle undertaken in this paper. The tunnel is of the open-jet and open-return type with a test section aspect ratio of 3:2 complete with full width moving ground plane (MGP), platen suction and upstream boundary layer suction. More details of the layout and characteristics of the tunnel can be found in extensive detail in [22, 23]. **Figure 2** shows the salient features of the tunnel. The test section is located within a large plenum chamber (not featured in the figure).
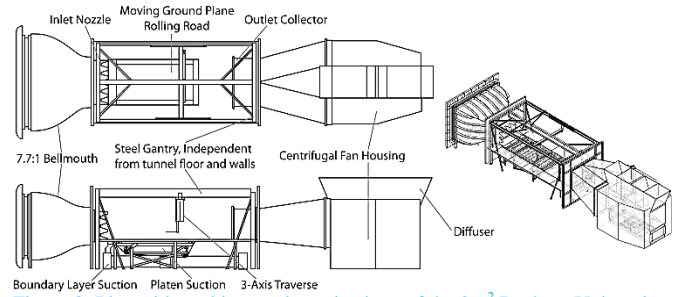
Figure 2: Plan, side and isometric projections of the 2m² Durham University wind tunnel highlighting some of the salient features [6].

Measurement Techniques

Balance Force Measurements

For the measurement of vehicle forces the model was fitted with an internal 6-component balance, with repeatability of ±0.002 on C_D and ±0.008 on C_L connected to a bank of Fylde FE-579-TA strain gauge bridge transducer amplifiers.

Surface Oil Flow-Visualisation

Surface oil flow-visualisation is a very beneficial technique for examining a local flow-field. Using flow visualisation, areas of recirculation, reattachment, separation, high vortical-flow and general flow direction could all be easily identified [24].

For this investigation, the technique involved the use of an orange UV-reactive powder mixed with kerosene (often paraffin) in order to produce a very low viscosity liquid. Coating the rear window region allowed the flow-field characteristics to be determined. By running wind-on for around five minutes the kerosene was allowed to evaporate, during which time the mixture entrained onto the surface airflow. Thus, evidence of the surface flow was left behind in the form of varying concentrations of the powder, now attached to the surface.

Finally, examination using a UV light allowed very subtle details to be identified and photographed for later analysis.

Particle Image Velocimetry (PIV)

Particle image velocimetry (PIV) is a non-intrusive measurement technique enabling the visualisation of a flow-field. It is not restricted by reverse flow regions and as such provides valuable information regarding the direction and magnitude of the velocity of the entire fluid flow. Part of the work in this paper was in relation to obtaining successful PIV measurements within a large working section, hence it will be discussed briefly here. More detailed information regarding PIV can be found in [25, 26, 27].

Seeding

The flow was seeded using a 40 nozzle seeder by ILATEC [27] which holds a reservoir of Di (2-ethylhexyl) Sebacate (DEHS). This fluid is atomised by the nozzles, fed by compressed air, and dispersed as a "fog" or "smoke" into the flow. The particle size is reported to be of the order of one micron for this seeder. This ensures a small enough particle to entrain onto the fluid correctly, without buoyancy effects affecting the path, but with large enough size to be detectable by at least two pixels in the camera field-of-view.

The seeder was connected to a purpose designed smoke-rake. This comprised of four copper pipes with 2mm diameter holes drilled 15 mm apart to allow high-density seeding in areas of interest and 25 mm spacing for low-density seeding around all other areas. Seeding intensity was controlled via the inlet air-pressure for the seeder and by temporary sealing of unwanted holes in the smoke-rake. It was important to balance the level of seeding as excessive smoke in the flow can cause a weakening of the image (due to distortion from smoke not in the laser plane) and also as the image can lose the distinct peaks necessary for cross-correlation.

The Laser

An Nd: YAG laser is a high-powered crystalline solid-state laser which is optically pumped via a high-intensity flash-lamp. The laser used in this investigation produced a high-intensity 120 mJ beam, visibly green of wavelength $\lambda = 532$ nm.

The purpose for using a dual-head laser was that in order to detect particle movement, but not allow signal drop-out at the same time, two images are required of the order of microseconds apart. As a result, two optical-cavities are needed as the laser would not have enough time to charge up for the second flash. More information on Nd: YAG lasers can be found in Silfvast [25].

Beam Delivery

The Durham University PIV Periscope, shown in **Figure 3**, was used as part of this work. This is a 90° bend which protrudes from a slot into the floor of the wind tunnel and allows for a high-quality high-reflectance mirror (98%) to be mounted onto a rapid prototyped cap.
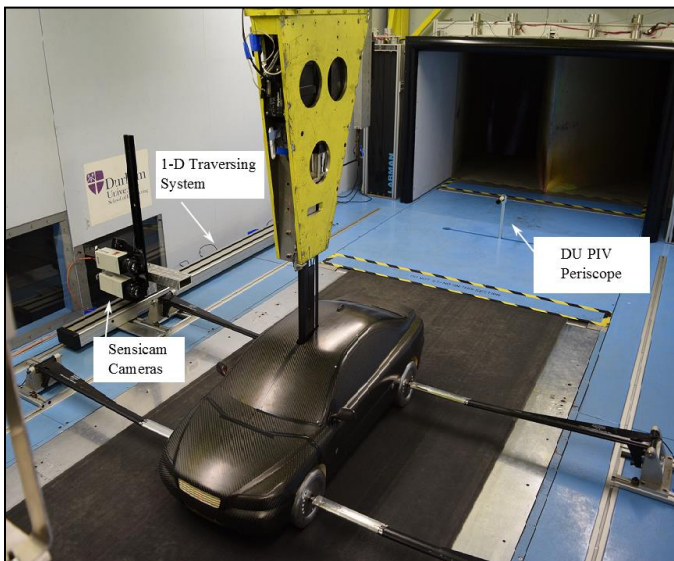

Figure 3: PIV set-up illustrating position of cameras, 1-D traversing system and Durham University's PIV periscope.

Although overall the images produced post-filtering vector field validity in excess of 90%, the periscope allowed a blockage of only 0.2% and delivered a beam within 95% of the overall intensity capacity of the beam.

Light - Sheet Optics

Once the laser beams were focused, coincident and co-linear, a set of light-sheet optics were used, essentially comprising a focusing lens followed by a cylindrical lens in order to disperse the sheet into a very thin diverging plane. It was vital to keep the beam from diverging too much otherwise laser intensity was wasted in the interrogation region. Finally, in order to have highly visible particles, it was also important to have the focal point at or near the area of interest.

Cameras

In order to double the size of the image frame, two Sensicam cameras were utilised, each with a Peltier-cooled CCD which was 1280×1024 pixels in size. The total instantaneous capture measured 180×350 mm. The cameras were grey-scale and could obtain 12-bit images allowing high fidelity in shading. This allowed precise representations of the particles in the flow to be captured in the images.

In addition, with the aim to allow further detail of the wake to be obtained, the cameras were placed on a one-dimensional traversing system which could be moved allowing both cameras to remain focused on the laser plane. This is shown in **Figure 3**.

The longitudinal plane (x-z) which describes the vertical centreline of the vehicle was used. For this study this was the most commonly used plane as the image quality was high and wake structures could be identified as well as allowing useful comparisons with CFD work.

Calibration Procedure

A calibration image was captured for the purpose of the analysis stage. In this investigation, this was achieved by a grid of squares, spaced 10mm apart, with every 50 mm being denoted by an 8 mm diameter circle. This could be detected by the VidPIV software when applying the calibration grid allowing it to "snap" to the photographed points. The calibration board positioned behind the Volvo S60 model is shown in **Figure 4**. A calibration image had to be taken for all camera and laser positions tested.
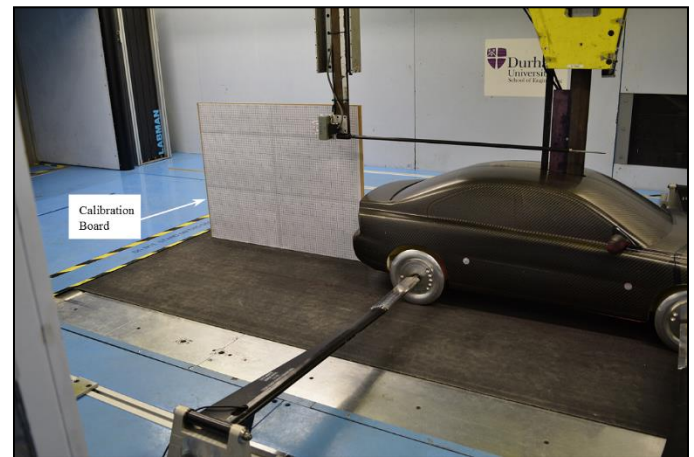

Figure 4: Calibration board used, in order to capture calibration image.

Timing and Synchronisation

The PIV synchroniser made by ILA [27] was used in this instance and controlled manually rather than by software interface. It was

found that more light intensity could be found by manually adjusting the settings as opposed to using the pre-defined laser-strength parameters in the software. The pulse energy setting was adjusted to 185 μs which allowed maximum light intensity to be achieved. Charging for longer than this resulted in either no further gain or a reduction in light intensity in extreme cases.

The pulse distance or image pair separation was measured empirically as being optimised around 20-30 μs, for an image width of around 300 mm with a free stream velocity of 25 m/s. This was sufficient to allow velocities to be tracked without pixel-locking.

The delays were set to zero and the camera width (triggering separation) was calculated automatically by the synchroniser's firmware. The remaining parameter, pulse frequency, was set at 4 Hz as higher frequencies resulted occasionally in misfires and unusable "dead image pairs" whereas lower frequencies extended the test period. Finally, for each test case 500 image pairs were recorded and processed. It was important to collect a high number of image pairs as possible in order to obtain high averaging quality.

Numerical Method

Numeric Volvo S60 models

Two vehicle configurations were chosen to be investigated in CFD. The first one was the full scale 2010MY Volvo S60, while the second one was a 30% scale model S60 representing a 2003MY vehicle. Both used numerical models were fully detailed, with representative engine bay and underbody, and can be seen in **Figure 5**.
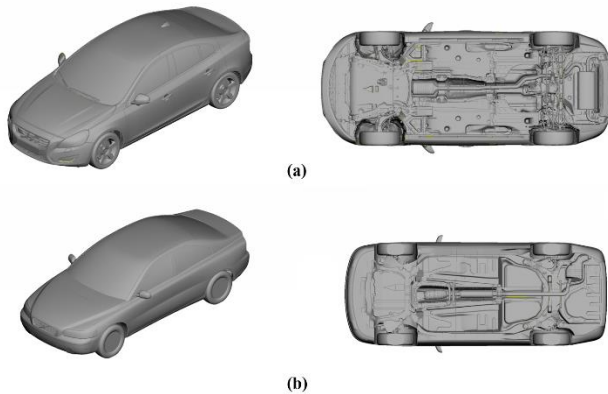

Figure 5: Numerical models with open cooling and detailed underbody (a) 2010MY Volvo S60, (b) 2003MY 30% Volvo S60.

Scale model

For the 30% scale model, two different test configurations were investigated as presented in **Table 1**.

Table 1: Configuration overview tested in CFD with description.

Test Case	Description
Baseline	V_{tunnel} = 25m/s, MGP&RW = 25 m/s, No Antenna
Baseline with Antenna	V_{tunnel} = 25m/s, MGP&RW = 25 m/s, With Antenna

The overall dimensions of the numerical box-shaped wind tunnel are 22 m × 5.4 m × 2.7 m in length, width and height respectively. A

representation of the wind tunnel with the relative position of the vehicle to its length is given in **Figure 6**. The distance of the model to the inlet and the outlet is ~5 L and ~10 L respectively, with L equal to the vehicle's length.
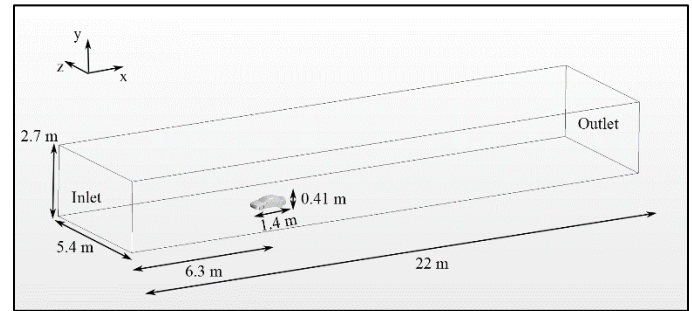

Figure 6: Numerical wind tunnel with relative vehicle position.

The simulations were performed in Star-CCM+, using a steady-state k-ω SST turbulence model. Since the model wheels were smooth, with no tyres or rims, wheel rotation was modelled using a moving wall boundary condition. For the mesh, 14 prism layers with a total thickness of 4 mm were used on the upper body, while 4 prism layers were built on the underbody and in the engine bay. This resulted in a mesh consisting of 160 million volumetric cells, with upper body y^+ < 1.

Full-scale model

For the numerical simulations of the full-scale model, the approach previously described in [26] was used. The simulations were performed on a fully detailed model in Star-CCM+, where a steady state RANS approach was used with a realizable k-ε turbulence model. Wheel rotation was modelled using a moving wall boundary condition and MRF zones in between the spokes of the rims. The volume mesh consisted of 96 million cells, with 3 prism layers of a total height of 7 mm, which resulted in upper body y^+ values in the range between 30 and 150.

Results

Limiting Streamline Pattern

Initially the limiting streamline pattern shall be investigated. The pattern obtained from paint visualisation on the model scale is compared with CFD simulations. Additionally, the limiting streamline pattern for the full scale S60 is presented and discussed.

The wind-tunnel model was supported by an overhead strut. Hetherington and Sims-Williams [28] investigated the interference effect of this strut and its influence onto the flow field of a notchback vehicle. The main change they found in the structures was that the flow field of the investigated notchback vehicle became more symmetric with only a small associated change in drag and lift at the rear of the vehicle. Drastic changes in the topology and the wake structure were not observed. The skin friction lines over the scale model, obtained paint visualisation are shown in **Figure 7**. It shows a symmetric pattern over the rear end, with two vortex structures right and left of the centreline.
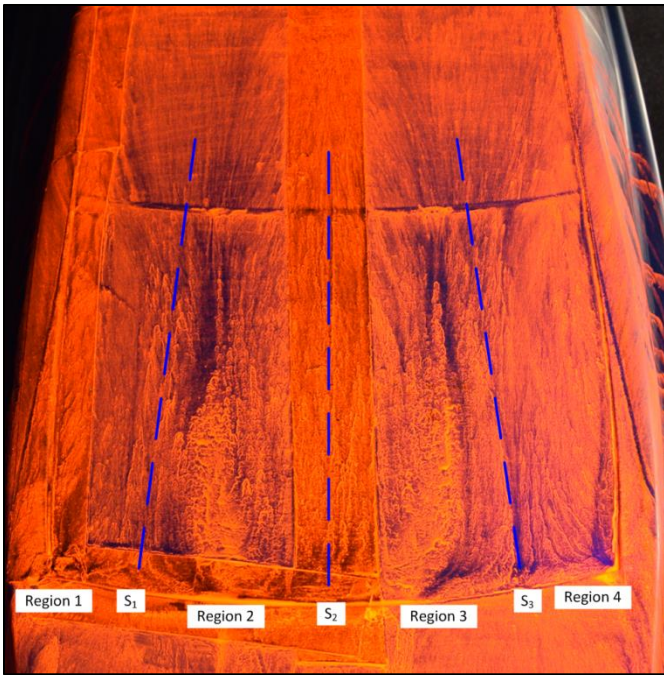
Figure 7: Limiting streamlines over the scale model.

Although it is hard to comprehend in the paint visualisation how the structures look exactly, it is possible to reconstruct them considering the saddle points S_1, S_2 and S_3. As S_1 pushes flow to the centre and S_2 pushes flow away from the centreline, another saddle point has to be created where the separatrixes from S_1 and S_2 meet (S_5 in **Figure 8**). The same applies between S_2 and S_3. Between the rear window and the trunk there is a small step in the geometry and the flow is pressed and cannot move further downstream. Between the separatrixes, foci have to develop to form a consistent limiting streamline pattern. An interpretation of the paint visualisation is given in **Figure 8.**
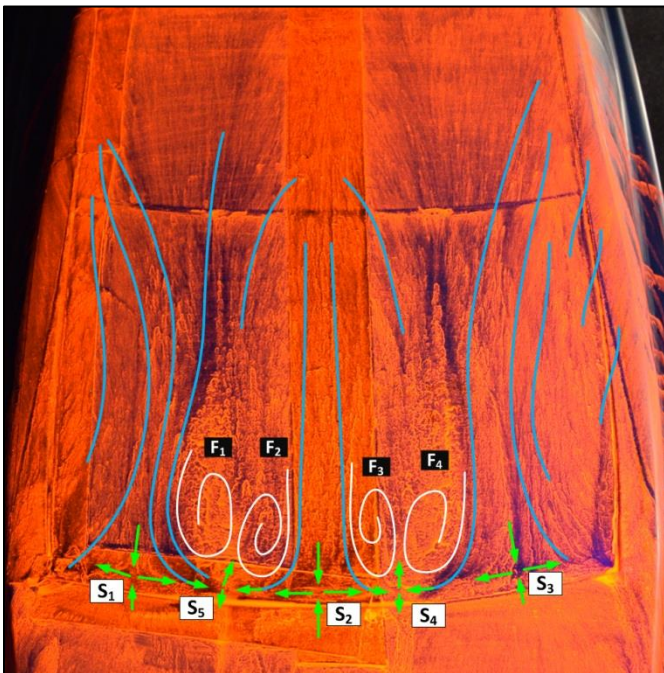

Figure 8: Limiting streamline pattern interpretation of the paint visualisation.

This pattern shall be compared with the limiting streamline pattern from CFD, presented in **Figure 9**. The flow over the roof seems to be aligned with the mean flow direction further upstream, before it starts moving inwards starting from the side edges of the roof (**Figure 9**). Contrary, in the experiment the flow upstream seems to have a more outward pointing pronunciation, and curving back to the mean flow direction reaching the rear window. From the roof edge and the C-pillar an inwards directed flow can be observed in the experiment, which agrees with the CFD simulation. A reason for this difference can be the overhead strut. It seems that the flow around the antenna cannot develop as shown in CFD due to outward pointing flow created by the strut.

Over the rear window, reaching the trunk, the pattern looks similar to the observations in the wind tunnel. At the lower edge to the trunk the saddle point S1 and S3 can be detected. S2 is slightly shifted upstream. But the exact location cannot be pointed out in the flow visualisation pictures. The CFD shows that the flow end is two counter rotating foci on each side of the centreline. This fits to the interpretation given in Figure 8. The exact shape of the foci could not be estimated in the experiment. However CFD shows that the inner two foci are smaller than the outer and located slightly upstream.

Figure 9: Limiting streamline pattern calculated in CFD for 30% Volvo S60 without the overhead strut

As it was mentioned earlier, the strut seems to change the limiting streamline pattern over the roof; therefore a picture from CFD with the strut is presented in **Figure 10**.

The outwash observed in the experiment is not as strong in CFD. But the foci pattern on the lower edge changed. The outer foci centre are located in the same way as for the no strut case. The foci shape on the top is stretched. The inner foci experience the biggest change. The foci centres are moved downstream, while the foci shape is more stretched in longitudinal direction.

In summary, it can be said that the overhead strut changed the pattern as it pressed downstream the inner foci. The overall pattern is not changed. The in-wash from the sides over the window is present in all cases and not affected by the strut. The main surface structures are created at the lower edge of the window and the interpreted saddle points can be found in the computed limiting streamline pattern.

These separation areas are located symmetrically to the left and right of the centreline and contain two counter rotating foci. These separation areas and the singular points are seen as the characteristic features of the rear end flow for this vehicle. Therefore it is proposed to use their location as a characteristic length scale. The ratio of the distance between the separation bubble centres and the window width, gives a value of 0.26 (no antenna) and 0.21 (with antenna) for CFD and 0.28 (with antenna) for the experiment.
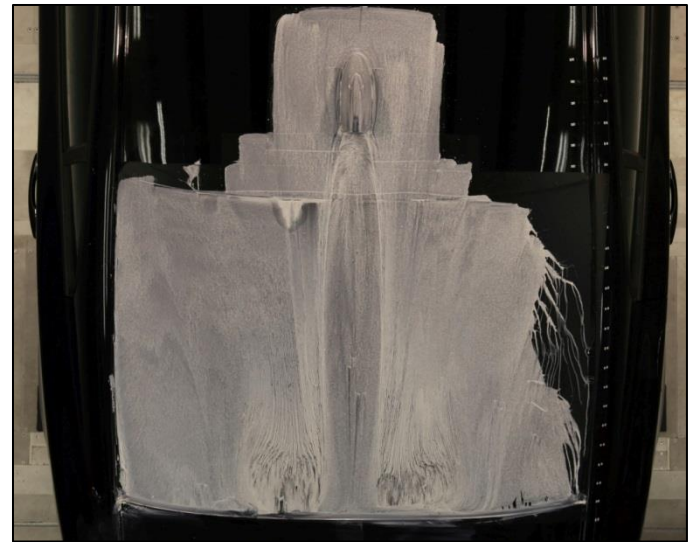

Figure 10: Limiting streamline pattern calculated in CFD for 30% Volvo S60 with the overhead strut

To show that the singular point pattern characterises the flow despite differences in the geometry and scale of the studied vehicle, the limiting streamlines over the rear window for the full scale car are shown in **Figure 11**.

Again a symmetric pattern can be observed with two separation areas at the lower edge of the window. Starting at the base of the antenna two separation lines are present. These are more distinct in the full scale visualisation than for the model scale. Reducing the amount of paint in the area of the separation bubbles (**Figure 11(b)**) reveals that in each bubble two vortices are present. In **Figure 11(c)** an interpretation of the limiting streamline pattern is given. As for the model scale, three main saddle points can be found at the lower edge where the flow is split up.

Additionally, saddle points occur above the separation bubbles which are not present in the scale model. The ratio between the distance of the separation bubble centres and the window width for this case resulted in a value of 0.27. This value is in the same range as the ratio calculated for the scale model case.

The limiting streamlines for the two vehicles (model scale and full scale) show very similar patterns regarding the occurring main structures and their position. Calculating a ratio to characterise the separation bubble positions with respect to the window width gives very similar values for model and full scale and seems to be a possible parameter which can be used for a more precise comparison between similar vehicle shapes.

(a)

(b)
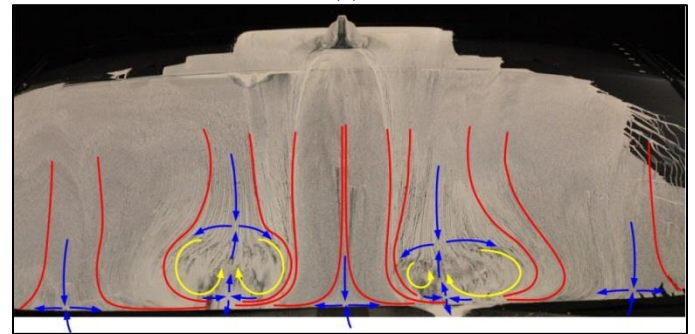
(c)

Figure 11: (a) Limiting streamline pattern over the rear window of a full scale car, (b) with reduced amount of paint in the area of separation bubbles, (c) graphical interpretation of the limiting streamline pattern.

Two-Dimensional Wake Analysis

XZ Planes for Baseline Case

In this section, a two dimensional wake analysis will be presented for the baseline case. In order to carry out this analysis, the PIV data as well as the steady-state CFD simulations were used for multiple y-positioned XZ planes. The y-positions (with respect to the 30% model scale vehicle) can be seen in **Table 2**.

Table 2: y-positions used for both PIV and CFD data.

y-position	Description
y_1	0 mm (Centreline)
y_2	-40 mm
y_3	-80 mm
y_4	-120 mm
y_5	-160 mm

For this analysis, it was decided to use four different parameters. Three of them are related to the length while one to the height of the base wake. These parameters are listed below and a schematic can be seen in **Figure 12.**

i. Horizontal distance between a base reference line (**B**) and the wake closing point denoted as (**S**).

ii. Horizontal distance between a base reference line (**B**) and the foci of the upper vortex structure (**F$_1$**).

iii. Horizontal distance between a base reference line (**B**) and the foci of the lower vortex structure (**F$_2$**).

iv. Vertical distance between the foci of the upper (**F$_1$**) and lower (**F$_2$**) vortices.
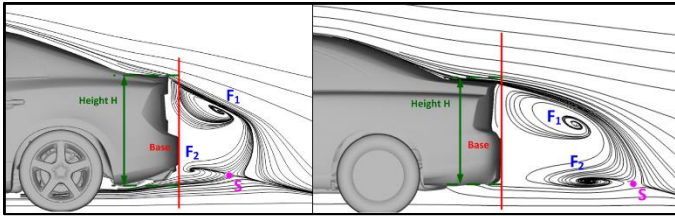

Figure 12: Schematic showing the parameters used for the 2D wake analysis study. (Left: Full scale S60 [2010MY], Right: Model scale S60 [2003MY]).

Before discussing the findings, it would be useful to mention that for PIV measurements and the y = -120 and -160 mm planes, it was decided not to plot the streamlines on the absolute velocity contour due to the poor resolution. The poor resolution for these two planes could be explained by the flow behaviour in that region. The flow is turning aggressively and as a result its components cross the measuring plane and alter the time-averaged result. Instead, velocity vectors plotted showing the generic flow features around the rear of the vehicle as it can be seen in **Figure 18** and **Figure 19**.

It would be useful to mention that upper figures represent experimental results while the lower ones, CFD results. Starting with the horizontal distance between the base reference line (**B**) and the wake closing point (**S**), it appears that the CFD steady state simulations over predict the wake length compared to the PIV measurements in the wind tunnel. This is consistent for all the y-positioned XZ planes. This is explained due to the fact that the

wheels and rear geometry generates large time dependent fluctuations in the wake, which are not correctly represented by the steady-state solver. However, it has to be mentioned that the steady state solution gives a correct impression of the occurring structures and their appearance. In addition, it is observed that the wake length does not change considerably by moving away from the centreline. This can be seen in **Figure 13**, **Figure 14** and **Figure 15**.
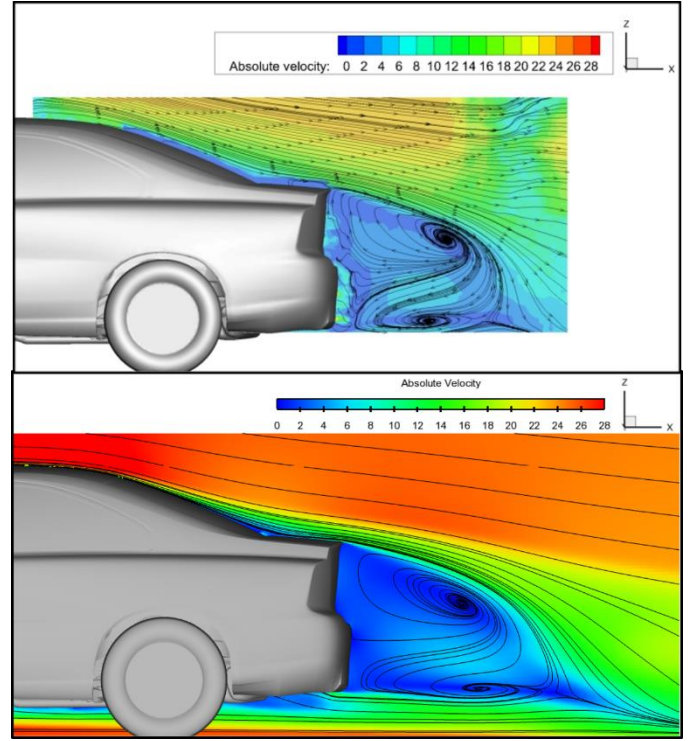

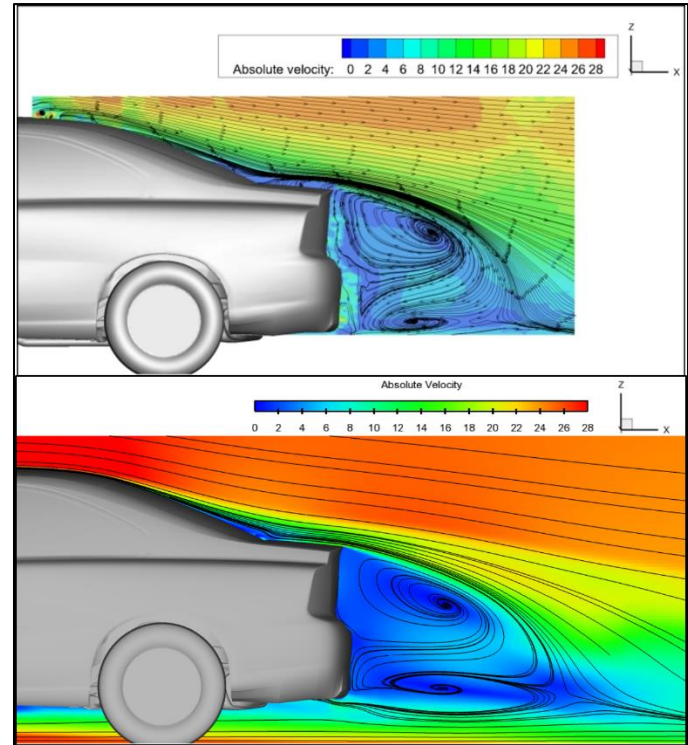Figure 13: Absolute velocity contours plotted with streamlines for $y_1 = 0$ mm.

Figure 14: Absolute velocity contours with streamlines for $y_2 = -40$ mm.

Moving on and analysing the horizontal distance between the base reference line (**B**) and the two foci of the upper (**F$_1$**) and lower (**F$_2$**) vortices, an alternate trend is noted. The distance to the upper vortex foci gets greater from the PIV measurements compared to the CFD simulations. However, for the lower vortex foci, CFD predicts a greater distance compared to the PIV measurements. This is visible in **Figure 13**. This behaviour is explained due to the underbody flow being over predicted from the steady-state simulations. Based on the fact that CFD simulations predict a greater distance to the wake closing point, it could be said that the lower vortex determines the closing point of the wake while the upper vortex influences the wake height as it will be discussed later. The last observation based on the distance to both vortex foci is that both vortices move closer to the vehicle's base region as one moves away from the centreline plane to $y_3 = -80$ mm. This is observed by comparing **Figure 13**, **Figure 14** and **Figure 15**.
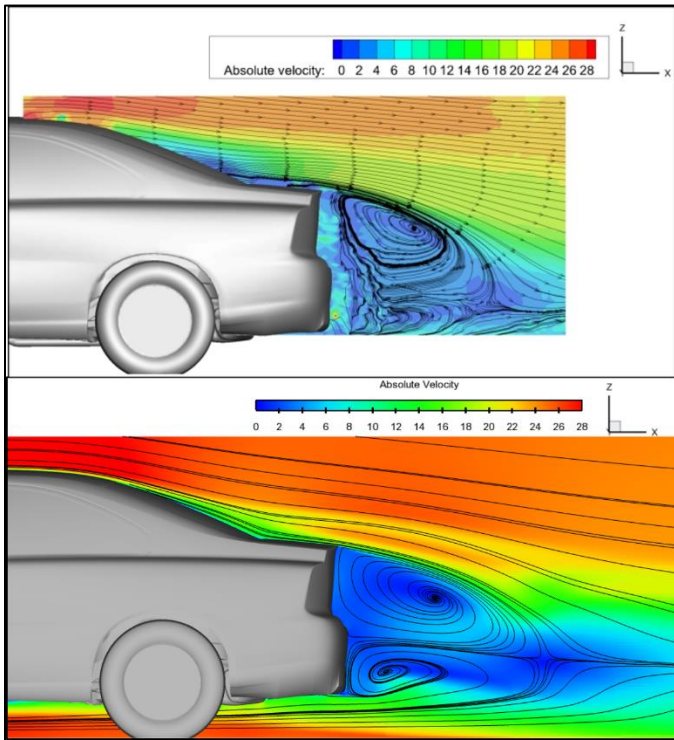

Figure 15: Absolute velocity contours with streamlines for $y_3 = -80$ mm.

Focusing only in CFD results, for the $y = -120$ mm plane, one could observe the presence of the C-pillar vortex as a high velocity region close to the mid-region of the C-pillar. In addition, the wake vortices seem to be similar in size and symmetric along the separatrix line. Finally the wake appears not to downwash compared to the centreline and $y_2 = -40$ mm planes. This could be explained by the size increase of the lower vortex, probably pushing the flow upwards compared to the other cases where the upper vortex is more dominant pushing the flow downwards. This is presented in the lower plot of **Figure 18**.

For the $y = -160$ mm, the presence of the C-pillar is once again visible but this time one could notice the high velocity region at the edge of the roof area. The most remarkable observation is the fact that the base vortices change the way of rotation at y_4 and y_5 compared to y_1, y_2 and y_3 positions. This change can be observed between $y=-110$ mm and $y=-115$ mm. The flow direction in both cases is anticlockwise, but for $y1$ to $y3$ the flow is directed towards the focus centre, while for $y4$ and $y5$ the focus is a source where the flow is emanated. It would be also useful to mention that the same

shift is seen for the full scale geometry as shown in **Figure 19**. In order to try explaining this phenomenon, further CFD streamline plots generated in the base region. The first observation was that the base flow is highly complex and asymmetric as it can be seen in **Figure 16**. The main features from this plane are the C-pillar vortices (top right and left) and the vortex which is a combination of wheel wake and flow coming from the waistline/bumper region (lower left).
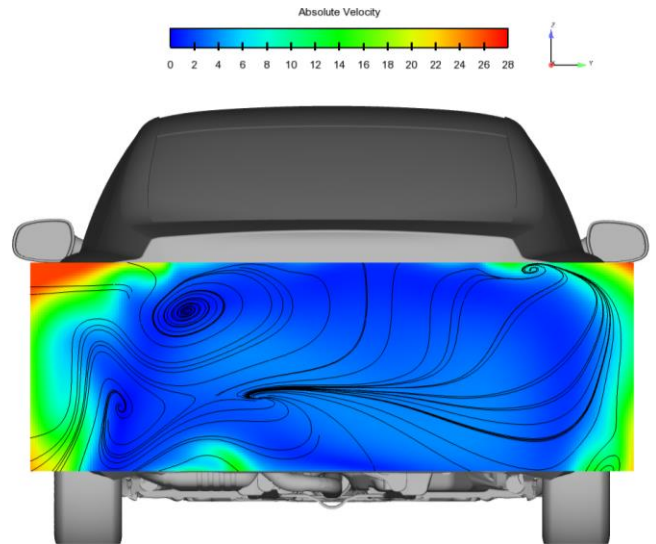

Figure 16: YZ absolute velocity contours with streamlines for x = 1757 mm.

Figure 17 shows the $y = -115$ mm together with the $z = 110$ mm plane. At the z-y plane a focus can be seen, too. It is assumed that actually a kind of ring vortex is created along the base region. The planes $y = -110$ mm and $y = -115$ mm are lying very close to the area, where the ring would have its vertical orientation. This leads to the assumption that the observed change of rotation direction is a graphical misinterpretation. In this region the flow has a significant y-component, which can also be seen in the PIV plots. Thus, a 2D representation of streamlines in this area causes a misleading link of the very weak velocity directions in x and z. According to the authors this would be the only viable explanation as one would expect the vortex to be continuous across the wake.
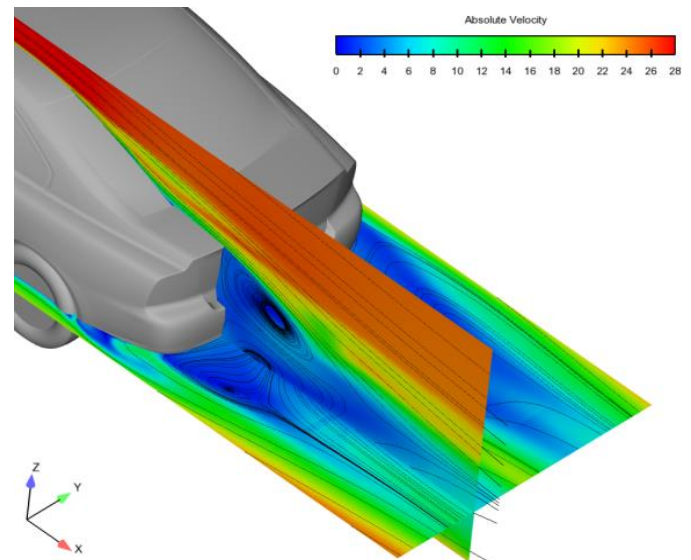

Figure 17: Isometric view of base wake structures (XZ and YZ planes).

Another interesting observation though is the considerable increase in size of the lower vortex compared to the upper one; resulting in the wake moving upwards, but also a movement of the wake closing point higher. Based on the analysis carried out with the wake parameters, the wake size decreases substantially, being the smallest compared to the other y-planes tested. This is shown in the lower plot of **Figure 18**.
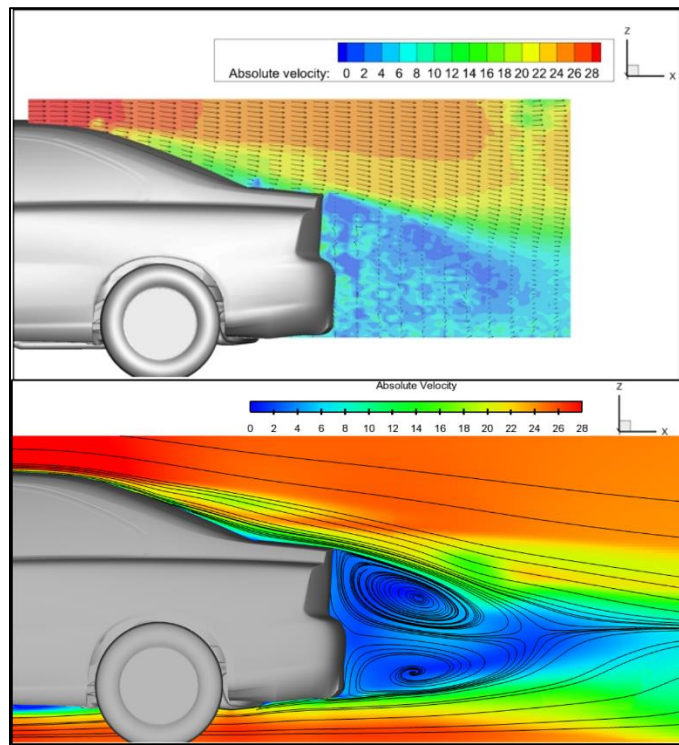

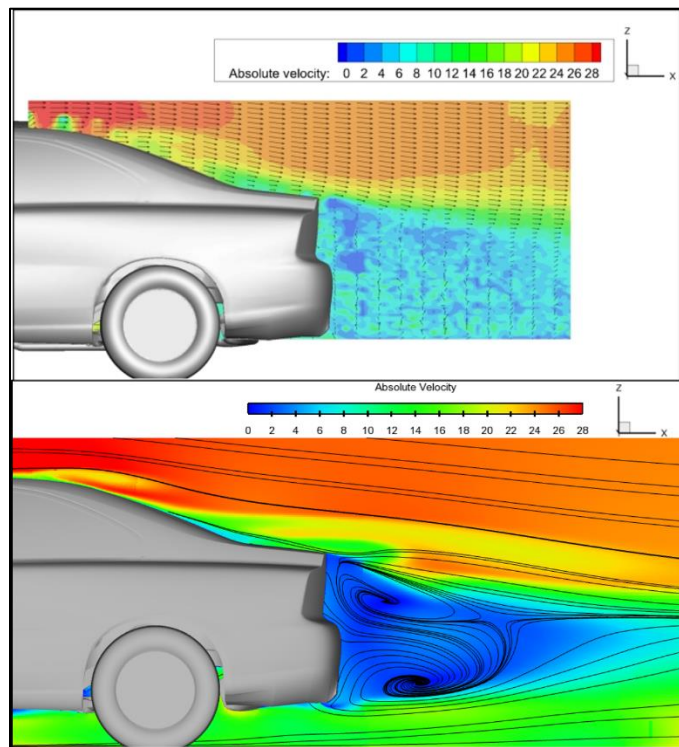Figure 17: Absolute velocity contours with streamlines for $y_4 = -120$ mm.

Figure 18: Absolute velocity contours with streamlines for $y_5 = -160$ mm.

Using the vertical distance between the foci of the upper (F_1) and lower (F_2) vortices, PIV measurements result in a greater wake height compared to the CFD simulations. This is an opposing trend compared to the wake length, where CFD simulation would over predict the length compared to the PIV measurements. Finally, for different y-planes, for PIV measurements, the wake appears to increase in height, but the opposite trend is noted for the CFD simulations. As discussed earlier the size of the upper vortex influences the wake height.

Looking at the CFD results, the size of the upper vortex seems to decrease as one moves away from the centreline plane. This in combination with the over prediction of the underbody flow from CFD (lower vortex increase in size and moves further away from the base compared to the upper one) would result in a smaller wake due to the flow moving upwards. This is a trend which was also noted from the full scale Volvo S60 (2010MY) CFD simulation results as presented in **Figure 19** for two y-planes.
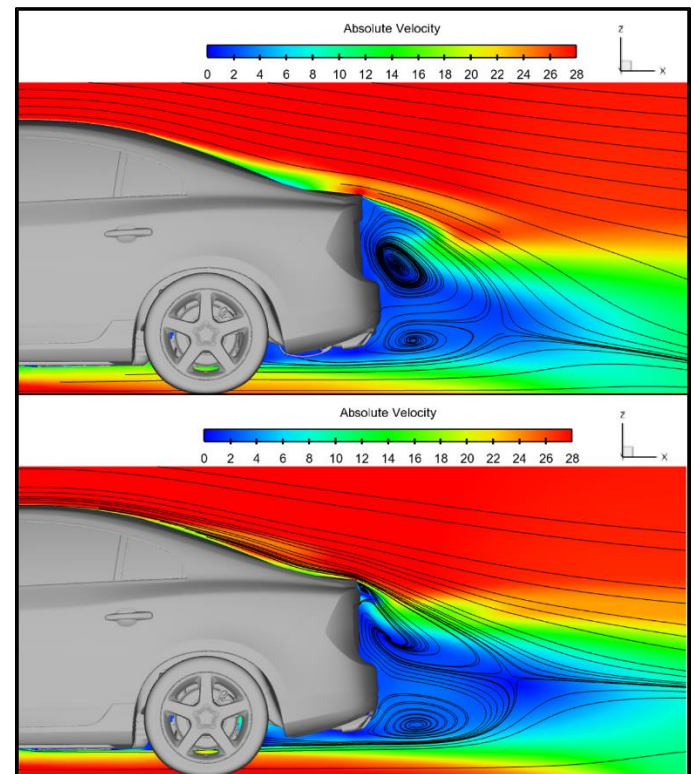

Figure 19: Absolute velocity contours with streamlines for full scale Volvo S60 (2010MY), for $y_3 = -80$ mm and $y_4 = -120$ mm planes.

Wake Length and Height Relation with the Base Height

The last thing done for this two-dimensional wake study was to try and qualitatively compare the wake structures from both PIV measurements and CFD simulations but also between the scale and full scale models.

In order to achieve that, a relationship between the wake height and base height was used. It would be useful to mention that the wake height was defined as the vertical distance between the upper and lower vortex foci and height as can be seen in **Figure 12**. The same thing was also tried with the wake length to vehicle's length relation. The wake length is defined as the distance from the base reference

line to the wake closing point. The equations used to calculate those ratios are presented below:

$$\text{Height Ratio}_{\text{wake/base}} = \frac{(F_1\text{-}F_2)_{\text{vertical}}}{H_b} \qquad (1)$$

$$\text{Length Ratio}_{\text{wake/vehicle}} = \frac{S}{L_{\text{vehicle}}} \qquad (2)$$

Studying the results of this analysis, it appears that for all the y-planes tested, the wake height is approximately 50% smaller than the vehicle's base height. In addition, it is noted that the CFD and PIV data match very well. Thus, independently of the y-plane used and the location of both upper and lower vortices, it seems that their distance remains constant. The same applies for the wake length, which was measured to be 20% of the vehicle's size for all y-planes with a similar good agreement between PIV and CFD measurements.

The same analysis using the same ratios was carried out for the full scale S60 vehicle in order to compare it with the mode scale results and see if there any similar trends. Results showed that for the height ratio, the values from the model scale matched the CFD simulations very well showing that the wake height is approximately 50% of the base height for the same planes considered. However, it is not possible to conclude the same for the length ratio. In that case, the ratio changes as we move away from the centreline compared to the model scale measurements where the values stay approximately the same. This could be explained due to the fact that the wake height is mainly influenced by the base height whereas the wake length is influenced more by the flow under the vehicle as well as other geometrical parameters such as the C-pillar radius, the rear window slope and the trunk deck length.

Three-Dimensional Flow Structures Study

Figure 20 shows the three dimensional development of the flow structures, visualized by the x-component of vorticity. The orange colored areas represent negative x-vorticity, while the blue areas represent positive x-vorticity. Over the rear window of the vehicle, four main vortices can be observed on each side. These are numbered as shown in **Figure 20(a)** below.
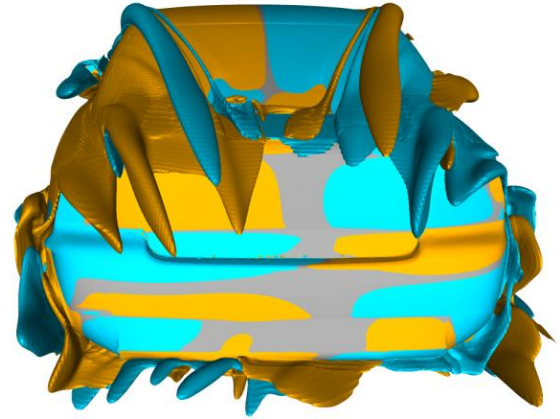
(b)

Figure 20: X-component vorticity (±250) in (a) Isometric view, (b) Rear view for the 30% scale model Volvo S60.

Starting from the A-pillar, vortex (1) is passing over the rear window. An interesting observation would be that a smaller vortex (3) which is generated upstream with vortex (1), after a while and close to the mid-roof region, it splits off from the main A-pillar vortex and travels downstream as a separate structure. This small vortex is lying off the surface and therefore does not leave any footprints in the limiting streamline pattern. Vortex (2) seems to be a structure emanating from the A-pillar as well, but rotating in opposite direction. Finally, over the C-pillar a vortex sheet is generated which results in vortex (4).

This is presented clearly in **Figure 21**, showing only the positive x-component vorticity denoted with light blue color. Without the counter-rotating A-pillar vortex (1) plotted, it can be seen that vortex (2) is formed upstream at the A-pillar. In addition, one could also note that on the right hand side of the rear window, the C-pillar generates vorticity which results in the vortex structure (4).
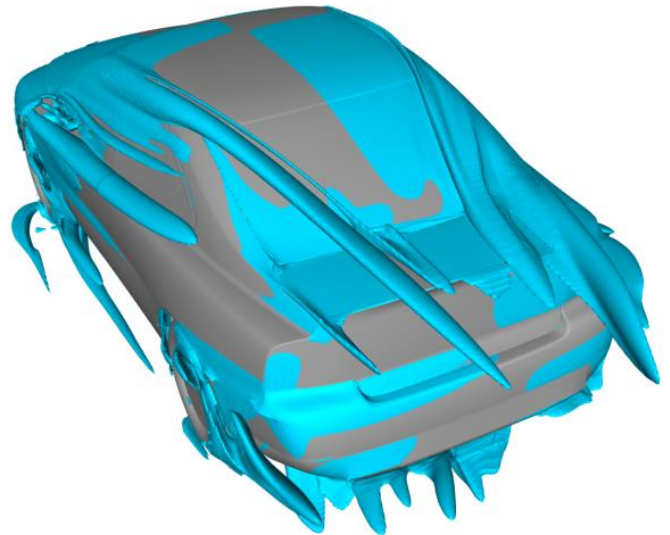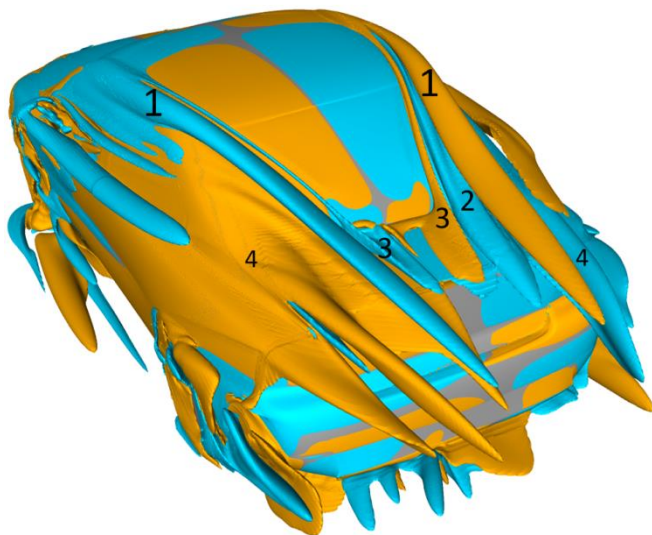

(a)

Figure 21: Positive x-component vorticity (+250) in isometric view for the 30% scale model Volvo S60.

The foci structures observed from the surface flow visualization study from both wind tunnel and CFD simulations appear not to result in strong vortices. At the lower region of the rear window, only weaker structures can be observed which seem like they merge with the smaller vortex (3).Vorticity iso-surfaces do not to give any indications of the observed wake vortices shown in the XZ cross planes (neither vorticity magnitude, nor y-vorticity). Thus, plotting total pressure iso-surfaces delivers more information regarding the wake structure.

Figure 22 shows a total pressure iso-surface at the -40 Pa level. It can be seen in **Figure 22(a)** that a ring is created around the base region. This corresponds to 2D observations discussed in the section called "XZ Planes for Baseline Case", where the upper and lower vortices are parts of this ring structure.

Figure 22(b) shows the iso-surface of a lower value together with the 2D Streamlines 115 mm to the left of the centreline. In this plot it is shown that the ring structure corresponds with the upper and lower 2D vortices observed in the XZ cross planes.
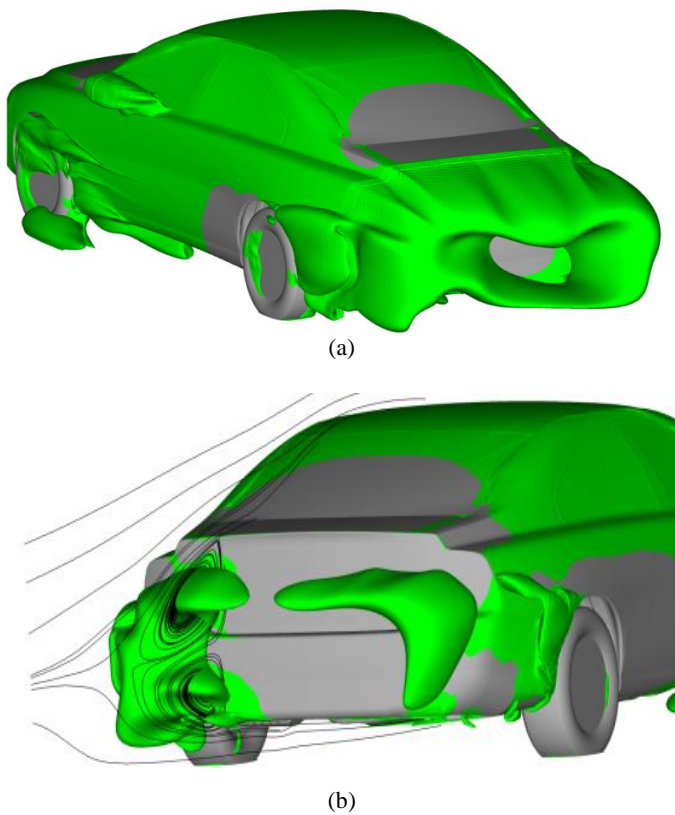

(a)

(b)

Figure 22: (a) Total pressure iso-surface (-40 Pa) and (b) total pressure iso-surface (-50 Pa) with streamlines at y = -115 mm.

Considering the fact that vorticity (or Q criteria) does not give any indications of the wake vortex but the total pressure distribution does, it leads to the following assumption: The C-pillar vortices are characterised by rotation, causing vortex drag. On the other hand, the wake vortices have much less rotation and are pressure losses which as a result cause pressure drag.

Force Coefficients Study

This section will briefly present a comparison on the force coefficients (drag and lift) gathered from CFD simulations and the Durham University's $2m^2$ wind-tunnel for the Volvo S60 [2003MY] without the antenna. In **Figure 23**, the drag and lift coefficients are presented for both methods. It would be useful to mention that the CFD force coefficients were averaged over roughly 5000 iterations.
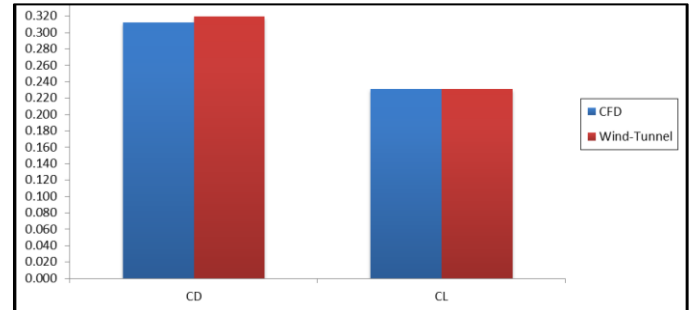

Figure 23: Force coefficients comparison for the 30% scale model Volvo S60 [2003MY] without the antenna for both CFD and $2m^2$ wind-tunnel.

As it can be seen, the correlation between the wind-tunnel and CFD simulations is good. The drag coefficient calculated in the wind-tunnel is 7 counts greater than in CFD, while the lift coefficient is the same for both methods used. The reasons for this greater drag coefficient in the wind-tunnel results could be the influence of the strut, however as Hetherington and Sims-Williams [28] concluded this effect would be small. Finally, the additional drag due to the wheel-stings was calculated to be approximately 5 counts and certainly would affect the overall drag value. Therefore, these results gave more confidence to the authors about the two methods used for the investigation of the scale model [2003MY].

Conclusions

The rear end geometry of road vehicles has a substantial influence on aerodynamic coefficients and as a result on energy consumption. Sedan or also called notchback geometries can produce particularly complex three-dimensional flow structures which can include substantial flow asymmetry according to literature. Nevertheless, the interrelation between the rear end geometry, flow asymmetry and aerodynamic drag for realistic vehicle shapes has lacked detailed investigation.

This work examines the flow structures of a 30% scale model of a Volvo S60 representing a 2003MY vehicle and a full scale 2010MY S60. A range of techniques are employed including surface flow visualisation, force measurements, Particle Image Velocimetry (PIV) over the backlight and trunk deck and CFD simulations.

Initially, the surface topology of the rear end (rear window and trunk deck) for both configurations is analysed, using surface flow visualisation to picture the skin friction pattern. The limiting streamlines for the two vehicles (model and full scale) show very similar patterns regarding the occurring main structures and their position. Calculating a ratio to characterise the separation bubble positions with respect to the window width gives very similar values for model and full scale and seems to be a potential parameter which can be used for a more precise comparison between similar vehicle shapes.

From the two-dimensional wake analysis carried out, it was concluded the lower vortex of the wake determines the wake closing point while the upper one influences the wake height. Moreover, as one moves away from the centreline, both vortices move closer to the vehicle, however the size of the lower one increases in size, pushing the flow upwards resulting in a shorter and smaller wake. This result also agreed to the full scale CFD simulations. Finally, trying something similar to what was tried with the separation bubbles of the rear window, the relationship between the wake length and height to the vehicle's length and base height respectively was studied for the 30% scale model. From this study, it was shown that the wake height is 50% smaller in size to the vehicle's base height while the wake length is 20% of vehicle's length, with a very good agreement between CFD simulations and PIV measurements and irrespective of the y-plane tested. For the full scale S60, the height relation matched the scale model, but not the wake length. The reasoning for this behaviour would be that the wake height is mainly influenced by the base height whereas the wake length is influenced more by the flow under the vehicle as well as other geometrical parameters such as the C-pillar radius, the rear window slope and the trunk deck length. Looking at the wake length and its correlation to the drag could be used to study geometric changes and their influence in the overall drag.

A study of the three dimensional structures using x-vorticity, identifies the main vortices from A and C-pillars. The structures emanating from the separation bubbles found in the limiting streamlines are weaker as expected. Then, the discussed vortices of the base wake are not visible in the vorticity plots. By showing total pressure iso-surfaces a ring vortex can be found in the base wake. It is concluded that the pillar vortices contain significant rotation which can be visualised by vorticity and result in vortex drag. Contrary, the wake contains mainly pressure losses with much less rotation, resulting in pressure drag. To conclude, both drag and lift coefficients generated from the CFD simulations and the wind-tunnel tests showed a good agreement for the 30% scale model Volvo S60 [2003MY] without the antenna.

The paper shows that singular points as characteristic features can be used to describe and discuss the flow pattern. Proposed characteristic length scales based on singular point locations can be a possibility to compare the flow field of different cases. It is shown that despite of the differences in scale, geometry and used tools the singular point pattern is comparable and characterizes the flow.

References

[1] G. W. Carr, Influence of rear body shape on the aerodynamic characteristics of saloon cars, vol. Report 1974/2, Motor Industry Research Association, 1974.

[2] T. Nouzawa, S. Haruna, K. Hiasa, T. Nakamura and H. Sato, Analysis of Wake Pattern for Reducing Aerodynamic Drag of Notchback Model, Warrendale, PA: SAE International, 1990.

[3] T. Nouzawa, K. Hiasa, M. Yoshimoto and S. Haruna, *Influence of Geometry of Rear part on the Aerodynamic Drag and Wake Structure of a Vehicle.*

[4] F. Chometon, Simultaneous Use Of Oil-Flow Patterns And Total Pressure Tomographies For A More Complete Understanding Of Flow Structures Around A Car, Warrendale, PA: SAE International, 1988.

[5] L. N. Jenkins, An Experimental Investigation of the Flow Over the Rear End of a Notchback Automobile Configuration, Warrendale, PA: SAE International, 2000.

[6] B. R. Gilhome, J. W. Saunders and J. Sheridan, Time Averaged and Unsteady Near-Wake Analysis of Cars, Warrendale, PA: SAE International, 2001.

[7] S. Depardon, J. J. Lasserre, L. E. Brizzi and J. Borée, ¼ Scale VehicleWake Pattern Analysis using Near-Wall PIV, Warrendale, PA: SAE International, 2006.

[8] A. P. Gaylard, J. P. Howell and K. P. Garry, Observation of Flow Asymmetry Over the Rear of Notchback Vehicles, Warrendale, PA: SAE International, 2007.

[9] D. Sims-Williams, D. Marwood and A. Sprot, "Links between Notchback Geometry, Aerodynamic Drag, Flow Asymmetry and Unsteady Wake Structure," *SAE Int. J. Passeng. Cars – Mech. Syst.,* vol. 4, 2011.

[10] S. R. Ahmed, "Influence of Base Slant on the Wake Structure and Drag of Road Vehicles," *Journal of Fluids Engineering,* vol. 105, no. 4, p. 429, 1983.

[11] S. R. Ahmed, "Wake Structure of Typical Automobile Shapes," *Journal of Fluids Engineering,* vol. 103, no. 1, p. 162, 1981.

[12] T. Nouzawa, K. Hiasa, T. Nakamura, A. Kawamoto and H. Sato, Unsteady-Wake Analysis of the Aerodynamic Drag of a Notchback Model with Critical Afterbody Geometry, Warrendale, PA: SAE International, 1992.

[13] C. Strangfeld, D. Wieser, H.-J. Schmidt, R. Woszidlo, C. Nayeri and C. Paschereit, "Experimental Study of Baseline Flow Characteristics for the Realistic Car Model DrivAer," SAE International400 Commonwealth Drive, Warrendale, PA, United States, 2013.

[14] D. Wieser, H.-J. Schmidt, S. Müller, C. Strangfeld, C. Nayeri and C. Paschereit, Experimental Comparison of the Aerodynamic Behavior of Fastback and Notchback DrivAer Models, Warrendale, PA: SAE International, 2014.

[15] J. Fuller and M. A. Passmore, "The importance of rear pillar geometry on fastback wake structures," *Journal of Wind Engineering and Industrial Aerodynamics,* vol. 125, pp. 111-120, 2014.

[16] Firoz Alam, Simon Watkins, Gary Zimmer and Clive Humphris, "Effects of Vehicle A-pillar Shape on Local Mean and Time-Varying Flow Properties," 2001.

[17] G. T. Chapman and L. A. Yates, "Topology of Flow Separation on Three-Dimensional Bodies," *Applied Mechanics Reviews,* vol. 44, no. 7, p. 329, 1991.

[18] S. Bonitz, L. Larsson, L. Löfdahl and A. Broniewicz, "Structures of Flow Separation on a Passenger Car," *SAE Int. J. Passeng. Cars - Mech. Syst,* vol. 8, no. 1, 2015.

[19] L. M. Christoffersen, C. Landströ̈m and L. Lö̈fdahl, "Investigation of the Cooling and Underbody Flow Field on a Detailed Model Scale Passenger Car: Part 1—Cooling Flows and Reynolds Number Effects," 2009, pp. 297-304.

[20] L. Christoffersen, C. Landström and T. Walker, *A Wind Tunnel Study Correlating the Aerodynamic Effect of Cooling Flows for*

Full and Reduced Scale Models of a Passenger Car.

[21] L. Christoffersen, L. Löfdahl and A. Jönson, *Interference between Engine Bay Flow and External Aerodynamics of Road Vehicles.*

[22] D. B. Sims-Williams and R. G. Dominy, *The design of an open-jet wind tunnel for model testing.*

[23] D. B. Sims-Williams and R. G. Dominy, "The Design of a New Wind Tunnel for Vehicle Aerodynamics Research," 2002 .

[24] A. J. Sprot, "Open-wheel aerodynamics: effects of tyre deformation and internal flow," Durham University, 2013.

[25] W. T. Silfvast, Laser fundamentals, 2nd Edition, Cambridge University Press, 2008.

[26] A. Vdovin, L. Lofdahl and S. Sebben, "Investigation of Wheel Aerodynamic Resistance of Passenger Cars," *SAE Int. J. Passeng. Cars - Mech. Syst.,* vol. 7, pp. 639-645, 2014.

[27] I. L. A. GmbH. [Online]. Available: http://www.ila.de.

[28] B. Hetherington and D. B. Sims-Williams, "Support Strut Interference Effects on Passenger and Racing Car Wind Tunnel Models," SAE International400 Commonwealth Drive, Warrendale, PA, United States, 2006.

Contact Information

Mr. Charalampos Kounenis
Durham University, UK
charalampos.kounenis@durham.ac.uk

Mrs. Sabine Bonitz
Chalmers University of Technology, Sweden
sabine.bonitz@chalmers.se

Acknowledgments

Definitions/Abbreviations

B	Base reference line
CCD	Charged Coupled Device
C_D	Drag Coefficient
CFD	Computational Fluid Dynamics
C_L	Lift Coefficient
CO_2	Carbon Dioxide
DEHS	Di (2-ethylhexyl) Sebacate
F_1	Foci point 1
F_2	Foci point 2
H_b	Base height
L	Vehicle Length
MGP	Moving Ground Plane
MRF	Multiple Reference Frame
MY	Model Year
Nd:YAG	Neodymium-doped Yttrium Aluminium Garnet
PIV	Particle Image Velocimetry
RANS	Reynolds Average Navier-Stokes
RW	Rotating Wheels
S	Wake closing point
$S_{1...5}$	Saddle points
SST	Shear stress transport
UV	Ultraviolet light
x	Longitudinal distance
y^+	Dimensionless wall distance
$y_{1...5}$	XZ planes across the y-axis
λ	Wavelength